NeuroImage 254 (2022) 119167

Contents lists available at ScienceDirect

NeuroImage

journal homepage: www.elsevier.com/locate/neuroimage

A populational connection distribution map for the whole brain white matter reveals ordered cortical wiring in the space of white matter

Dongha Lee [a,b,1,*], Hae-Jeong Park [a,c,d,1,*]

[a] Center for Systems and Translational Brain Sciences, Institute of Human Complexity and Systems Science, Yonsei University, Seoul, Republic of Korea
[b] Cognitive Science Research Group, Korea Brain Research Institute, 61 Cheomdan-ro, Dong-gu, Daegu, Republic of Korea
[c] Department of Nuclear Medicine, Graduate School of Medical Science, Brain Korea 21 Project, Yonsei University College of Medicine, 50-1 Yonsei-ro, Seodaemun-gu, Seoul, Republic of Korea
[d] Department of Cognitive Science, Yonsei University, Seoul, Republic of Korea

A B S T R A C T

The white matter in the brain is composed of neural fibers that wire the cortical and subcortical brain systems. Considering the complexity in terms of interconnections of many neural populations within the narrow space surrounded by the folding walls of the gray matter, the brain requires a certain way of structured wiring. To explore the three-dimensional organization of wiring in an accessible manner, we focused on voxel-level wiring patterns in the white matter according to cortical distributions in which each voxel mediates the wiring. We constructed a voxel-wise connection distribution map from the whole white matter voxels to 360 cortical regions using probabilistic tractography of the 100 diffusion imaging data in the Human Connectome Project. We then explored the spatial organization of the fiber bundles at the white matter voxels in terms of the maximal and second maximal cortical connection labels and the local gradient and entropy of cortical connection density using the population connection distribution map. We presented dominant cortical connection labels, local gradient, and connection entropy for the most representative white matter regions, including the internal capsule, external capsule, corpus callosum, cingulum bundle, and uncinate fascicles, most of which were introduced in the current study. Those major tracts showed a gradient organization of connection distributions for individual voxels. This organized pattern, as reflected in the whole brain connection distribution map, could be established to optimize wiring in the entire brain within the physical space of the white matter.

1. Introduction

The white matter in the brain is composed of neural fibers that wire the cortical and subcortical brain regions, thus mediating functional integration across the whole brain (Park and Friston, 2013). To interconnect distributed regions within the narrow space surrounded by the folding walls of the gray matter, the brain requires a certain way of ordered wiring in a three-dimensional (3D) space. However, how axonal fibers structurally wire in a three-dimensional space has not been fully explored to date. In order to simplify the exploration of structured wiring in an accessible coordinate system, we focused on a voxel-level analysis in the white matter space because each voxel contains diverse fibers from the cortical or subcortical regions. Suppose we have the distribution of cortical connection labels at each voxel. In that case, we can characterize the spatial distribution of wiring in the white matter space and may uncover the structured wiring pattern in the brain.

Exploration of white matter fibers in the living human brain has been possible by the introduction of diffusion magnetic resonance imaging (MRI), which detects anisotropic water diffusion in the tissue (Basser et al., 1994). Since its introduction, numerous brain studies, such as those on schizophrenia (Kubicki et al., 2007; Park et al., 2004b), have been conducted based on voxel-specific tissue properties such as fractional anisotropy or diffusivity of the white matter, without consideration of the direct interconnections that each voxel mediates (Park, 2005).

As another approach to white matter analysis based on diffusion MRI, inter-regional structural connectivity among brain regions has been researched by constructing fiber streamlines using a fiber tractography technique and associating the whole-brain streamlines with the gray matter partitions (Park et al., 2004a). This macroscopic structural connectivity establishes human connectome research (Sporns, 2013), which expands our understanding of the brain's network structure (Bullmore and Sporns, 2012; Hagmann et al., 2007). However, most research on the connectome has been conducted in the abstract domain by counting fiber streamlines interconnecting gray matter brain regions without considering the physical white matter space that embeds these axonal fibers. How fiber bundles occupy the physical white matter space has rarely been researched.

To explore fiber organization within the entire white matter, we created a connection distribution map of the whole white matter voxels to 360 cortical regions from the diffusion MRI data of 100 subjects in the Human Connectome Project (Van Essen et al., 2012). In this map, voxels in the white matter space are characterized by the distribution of the

* Corresponding authors at: Department of Nuclear Medicine, Yonsei University College of Medicine, 50-1 Yonsei-ro, Seodaemun-gu, Seoul, Republic of Korea, Cognitive Science Research Group, Korea Brain Research Institute, 61 Cheomdan-ro, Dong-gu, Daegu, Republic of Korea.
E-mail addresses: donghalee@kbri.re.kr (D. Lee), parkhj@yonsei.ac.kr (H.-J. Park).
[1] These authors contributed equally to this work.

https://doi.org/10.1016/j.neuroimage.2022.119167.
Received 20 October 2021; Received in revised form 24 January 2022; Accepted 30 March 2022
Available online 2 April 2022.

Table 1
Demographic characteristics of 100 subjects.

	Male	Female
Gender	41	59
Age, Years	28.9 ± 3.7	30.1 ± 3.4
Ethnicity Not Hispanic/Latino	38 (92.7%)	54 (91.5%)
Hispanic/Latino	3 (7.3%)	5 (8.5%)
Height (feet)	70.9 ± 3.2	65.2 ± 2.3
Weight (lb)	192.7 ± 38.5	161.2 ± 37.1
BMI (height / weight)	26.9 ± 4.8	26.6 ± 5.4

connections with cortical regions that each white matter voxel mediates. This connection distribution map differs from previous white matter atlases, such as the ICBM-DTI-81 white-matter labels atlas (Mori et al., 2008; Oishi et al., 2008) and the JHU White-Matter Tractography Atlas (Hua et al., 2008). In those white matter atlases, each voxel is considered in terms of major fiber bundles to which the voxel belongs, not according to the distributed gray matter regions that the voxel mediates during interconnection.

Several studies have identified white matter voxels based on their connection distributions. Park et al. (2008) proposed a callosal connectivity population map in the mid-sagittal section of the corpus callosum according to each voxel's connectivity with 64 distributed cortical brain regions. Chao et al. (2009) expanded this precise callosal connection map using a probabilistic method that combined cytoarchitectonic parcellation and high angular resolution diffusion imaging. However, those studies were restricted to a part of the white matter regions and assigned each white matter voxel with the cortical label that the voxel primarily connected. However, they did not pay sufficient attention to the distribution of cortical connections at each voxel and its spatial distribution across the white matter.

From the connection distribution map, we also evaluated connection gradients and entropies of connections in the whole white matter space. The gradient measures how sensitively the connection distribution changes spatially. The entropy quantifies the amount of the spatial dispersion of white matter connections. To present the wiring structures, we analyzed the characteristics of connection distribution at the following major fiber bundles: internal capsule, external capsule, corpus callosum, cingulum bundle, and uncinate fascicles. We further argue that this connection distribution map supports structured white matter wiring with regard to gray matter.

2. Materials and methods

2.1. Data acquisition and processing

We used a total of 100 diffusion MRI and T1-weighted MRI pairs without any neurological or psychiatric disorders, drug-abuse in the Human Connectome Project (HCP1200) database (Van Essen et al., 2012). When the data was from the twins, only one of the twins was randomly included. The 100 dataset was composed of 41 males (aged from 22 to 35 years, mean age = 28.9, standard deviation (SD) = 3.7) and 59 females (aged from 24 to 36 years, mean age = 30.1, SD = 3.4). Among the HCP 1200 database, approximately 349 data satisfy the current criteria, but we chose only 100 data samples in the release order due to the high computational cost. Demographic characteristics of 100 subjects are summarized in Table 1. Using probabilistic fiber tractography, a hundred samples would be reasonable to construct a population connection distribution map for the narrow age ranged population when considering previous atlases with a deterministic approach. For example, ICBM-DTI-81 atlas was composed of 81 subjects (Mori et al., 2008).

The diffusion MRI data consisted of 4 runs with three shells of *b*-values (1000, 2000, and 3000 s/mm2). We used minimally preprocessed data with the following preprocessing steps: (1) intensity normalization across runs, (2) EPI distortion correction, (3) eddy current and motion correction, (4) gradient nonlinearity correction, (5) BEDPOSTX (Bayesian estimation of diffusion parameters obtained using sampling techniques) based on Gamma distribution model (Jbabdi et al., 2012) for the three different *b*-values to improve the estimation of fiber orientations.

To construct a structural connectivity matrix, we followed a conventional pipeline for probabilistic fiber tracking using the FSL toolbox (https://www.fmrib.ox.ac.uk/fsl) in the individual diffusion MRI space (Behrens et al., 2007). First, we coregistered the T1-weighted image to the non-diffusion weighted MRI image of each individual. To parcellate the individual brain, we then applied non-linear transformation of the HCP parcellation map using the DARTEL toolbox in SPM 12 (Ashburner, 2007). All voxels within the white matter (after segmentation using SPM12 available at https://www.fil.ion.ucl.ac.uk/spm/software/spm12) were used as seed voxels. Probabilistic fiber connections between a seed voxel and parceled target brain regions were estimated using PROBTRACKX (probabilistic tracking with crossing fibers) with the following parameters: 5000 random samples (thus, 5000 tracking) according to the orientation probability model for each voxel, 0.2 curvature threshold, 0.5 mm step length, and 2000 steps per sample. This probabilistic fiber tracking for all voxels (~300,000) within the white matter was accelerated by using Graphics Processing Units (GPUs) (Hernandez-Fernandez et al., 2019). Fiber tracking streamlines seeded from each white matter voxel and projected to the target cortical gray matter were used to estimate structural connectivity (Johansen-Berg et al., 2004; Li et al., 2012). We used a cortical gray matter parcellation map of 360 subregions, provided in the HCP database (Glasser et al., 2016).

It should be noted that fiber streamlines estimated by the computational approach on diffusion imaging are not axonal fibers but indicate the probabilistic approximation of the neural pathways. Also, the counts of streamlines are not the actual counts of axonal fibers but are simply probabilistic metrics with a given number of multiple tracking from a seed.

We constructed a structural connectivity matrix by counting the number of streamlines from each voxel to all the brain regions. We call the structural connectivity matrix [V white matter voxels × R regions] of individuals an individual connection distribution map (iCDM), which is a vector map composed of $R = 360$ three-dimensional volumes. The connection probability at each white matter voxel to a cortical brain region was defined by the ratio of the number of streamlines projected to the cortical regions from the voxel versus the total number of streamlines generated at the voxel. The iCDMs were spatially normalized into a template space using the DARTEL transformation derived from individual T1-weighted MRI to the ICBM (International Consortium for Brain Mapping) template. A population connection distribution map (pCDM) was obtained by averaging the normalized iCDMs.

Based on the pCDM, we constructed a connection label map (pCLM), which was created by assigning the cortical label having the highest probability of connection from each voxel v to 360 cortical regions R in the pCDM.

$$pCLM(v) = \arg\max_{r \in R} pCDM(v, r) \quad (1)$$

We also constructed a second connection label map based on the second-highest probability of connections (see Supplementary Fig. 2).

From the pCDM, we generated a populational connection local-gradient map (pCGM) and a population connection entropy map (pCEM). The pCGM was defined by a connection local-gradient index which refers to one minus Vogt-Bailey (VB) index (1−VB index) at each voxel. The VB index refers to the normalized second smallest eigenvalue (called the algebraic connectivity by Fiedler, 1973) of the graph Laplacian for the affinity (or similarity) matrix among neighbors at each region (Bajada et al., 2020). For this, we computed a local affinity matrix (A) at each voxel that was defined by dot products between all pairs of connection distributions of neighbor voxels ($N \times R$, where $N = 33$ is the total number of neighboring voxels including the voxel and $R = 360$

is the number of cortical regions).

$$A(i,j) = \sum_{r=1}^{R} pCDM(v_i, r) * pCDM(v_j, r) \quad (2)$$

The graph Laplacian L of the local affinity matrix A is defined as a diagonal degree matrix D minus the affinity matrix A as

$$L = D - A \quad (3)$$

Laplacian matrix L has eigenvalues $\lambda_1 \leq \lambda_2 \leq \cdots \leq \lambda_N$ after generalized eigenvalue decomposition

$$L\boldsymbol{v} = \lambda D\boldsymbol{v} \quad (4)$$

, where $\boldsymbol{v}$ is eigenvectors to the N eigenvalues. VB index was defined with the second smallest eigenvalue (λ_2) as the smallest eigenvalue (λ_1) for the positive semi-definite graph Laplacian is zero (Bajada et al., 2020). The VB index characterizes a white matter voxel whether it has at least one sharp change in the connection distribution (low VB index around 0) or contains only graded changes in the connection distribution (high VB index around 1). To consider high values for voxels with sharp changes (or gradients) in the relationship to each other among neighbors, we computed connection local-gradient map by one minus VB index at each voxel v, defined below:

$$pCGM(v) = 1 - \frac{\lambda_2}{\sum_{i=2}^{N} \lambda_i} \quad (5)$$

For pCEM, we computed the entropy of the connection distributions (across 360 cortical regions) at each voxel from the pCDM with the following equation:

$$pCEM(v) = -\sum_{r \in R} log\ pCDM(v,r)\ pCDM(v,r) \quad (6)$$

, $pCDM(v,r)$ indicates connection probability between a voxel v and target cortical region r in all target regions R.

3. Results

Fig. 1 displays examples of connection probability distributions at the voxels within the corticospinal tract. The distribution patterns of cortical connections (360 cortical gray matter regions) change along the corticospinal tract (voxels 1–3) (Fig. 1A). Fig. 1B and C display the connection (local-) gradient and entropy maps, respectively. High connection gradient voxels indicate where multiple streamlines diverge (Fig. 1B). The high entropy regions mediate diverse cortical connections rather than focused connections (Fig. 1C).

The pCLM, pCGM, and pCEM of the whole white matter are presented in Supplementary Figs. S1–S4. Fig. 2 shows a representative example of the pCLM, pCGM, and pCEM for the internal and external capsules. The pCLM (Fig. 2B) derived from the highest probability of connection to 360 cortical regions (shown in Fig. 2A) differs from the ICBM-DTI-81 white matter label atlas (see Fig. 2C). The ICBM-DTI-81 atlas assigns each voxel with the major white matter pathway label, whereas the pCLM assigns a most probable cortical region.

The pCLM also shows that white matter has a spatially organized connection structure according to the three-dimensional location of target cortical regions. For example, the anterior limb of the internal capsule was parceled into two orbital and polar frontal cortical areas (10pp, 10d) (Fig. 2D). The posterior limb of the internal capsule has more granular subdivisions than the anterior limb. It comprises ordered streamlines that mediate the anterior cingulate and medial prefrontal cortex (9m), dorsolateral prefrontal cortex (8BL, SFL), supplementary motor area (6ma, 6mp), primary motor cortex (4), primary sensory cortex (1), superior parietal cortex (7Am), and posterior cingulate cortex (POS2). The ordered granularity is prominent in the local gradient map (Fig. 2E). The external capsule also has an ordered set of streamlines according to positions of the cortical regions that the streamlines mediate. In the external capsule, the anterior part is composed of streamlines that mainly mediate the anterior insula areas (PoI1) and the posterior insula areas (PoI2). The streamlines at the posterior part of the external capsule are subdivided into connections with the supplementary motor area (6mp), the primary motor cortex (4), and the primary sensory cortex (3b). All cortical regions that voxels in the internal and external capsules primarily connect are displayed on the cortical surface in Fig. 2G.

Fig. 3 presents connection maps for the corpus callosum (CC), which show a similar subdivision to a cell-type based gross subdivision reported in Witelson (1989). The interhemispheric streamlines at the CC show a spatial order from the anterior to the posterior and from the ventral to the dorsal part. Streamlines passing through the genu and rostrum mediate interhemispheric connections for the anterior cingulate and medial prefrontal cortex (9m, 10v, 10r, 25), orbital and polar frontal cortex (10pp, 10d), and dorsolateral prefrontal cortex (9a), whereas streamlines crossing the rostral body are only engaged in connecting the dorsolateral prefrontal cortex (8Av, 8BL). Callosal fiber streamlines, running through the anterior and posterior midbody, connect the cross-hemisphere dorsolateral prefrontal cortex (SFL), supplementary motor areas (6ma, SCEF, 6mp), and primary motor cortex (4). Streamlines of the isthmus connect the somatosensory cortex (1, 3b), paracentral lobule (5m, 5L), and the superior parietal cortex (7AL). Streamlines passing through the splenium connect the superior parietal cortex (7Am, MIP), posterior cingulate cortex (POS2, RSC), early visual cortex (V3), and primary visual cortex (V1) (Fig. 3A and B).

A high connection gradient was located mainly between the anterior/posterior cingulate cortices and other regions (Fig. 3C and D). In those areas, streamlines rapidly change along with the spatial location of the target cortical regions. In contrast, a low gradient was found in the ventral parts of the rostral body, midbody, and ventral-posterior splenium. The anterior splenium showed a high entropy of connection distribution, while the ventral parts of the genu showed relatively low entropy of interhemispheric connections (Fig. 3E and F).

Fig. 4 presents the populational connection labels, gradients, and entropy maps for the cingulum bundle (CB). In the pCLM, streamlines passing through the anterior CB interconnect the anterior cingulate and medial prefrontal cortex (25, 10v) and orbital and polar frontal cortex (10d), whereas the posterior CB mediates mainly the posterior cingulate cortex (RSC, POS1, v23ab, 7m) (Fig. 4A, top panel). The pCGM shows a high local connection gradient at the voxels corresponding to the middle and anterior cingulate and the medial prefrontal cortex (Fig. 4A, middle panel). The gradient was higher in the ventral-anterior part and the ventral-lateral part of the CB than in the posterior part of the CB or the dorsal-medial part of the CB (middle panel). In contrast to the local gradient, entropy was generally high at voxels in the CB except for the posterior part (Fig. 4A, bottom panel). Fig. 4B displays connection labels of the CB and cortical connections at two exemplary voxels on the cortical surface.

Fig. 5 shows populational connection maps of the uncinate fasciculus (UF). In the pCLM, streamlines passing through the anterior portions of the temporal lobe project to the insular and frontal opercular cortex (POI1, AAIC, Pir), TGd, and V1. Streamlines that pass through the frontal lobe project to the inferior frontal cortex (47l, p47r, 45, IFSa), orbital and polar frontal cortex (a47r), and insular and frontal opercular cortex (FOP5) (Fig. 5A, top panel). Connection labels of the UF and the cortical connections at two sample voxels in the temporal lobe and frontal lobe are displayed on the cortical surface (Fig. 5B).

Fig. 6 summarizes the spatial order of the wiring in the three-dimensional space. The spatial wiring order in the cortical connections within the white matter exists in the three principal axes: anterior-posterior, dorsal (superior)–ventral (inferior), and lateral-medial, respectively. Anterior-to-posterior and dorsal-to-ventral directional segregations were evident in the CC and CB. Dorsal-to-ventral segregations can be found in the UF. Anterior-to-posterior and lateral-to-medial segregations were dominant in the internal and external capsules.

Fig. 7 presents the connection label, gradient, and entropy maps in comparison with the tract-based spatial statistics (TBSS) skeleton

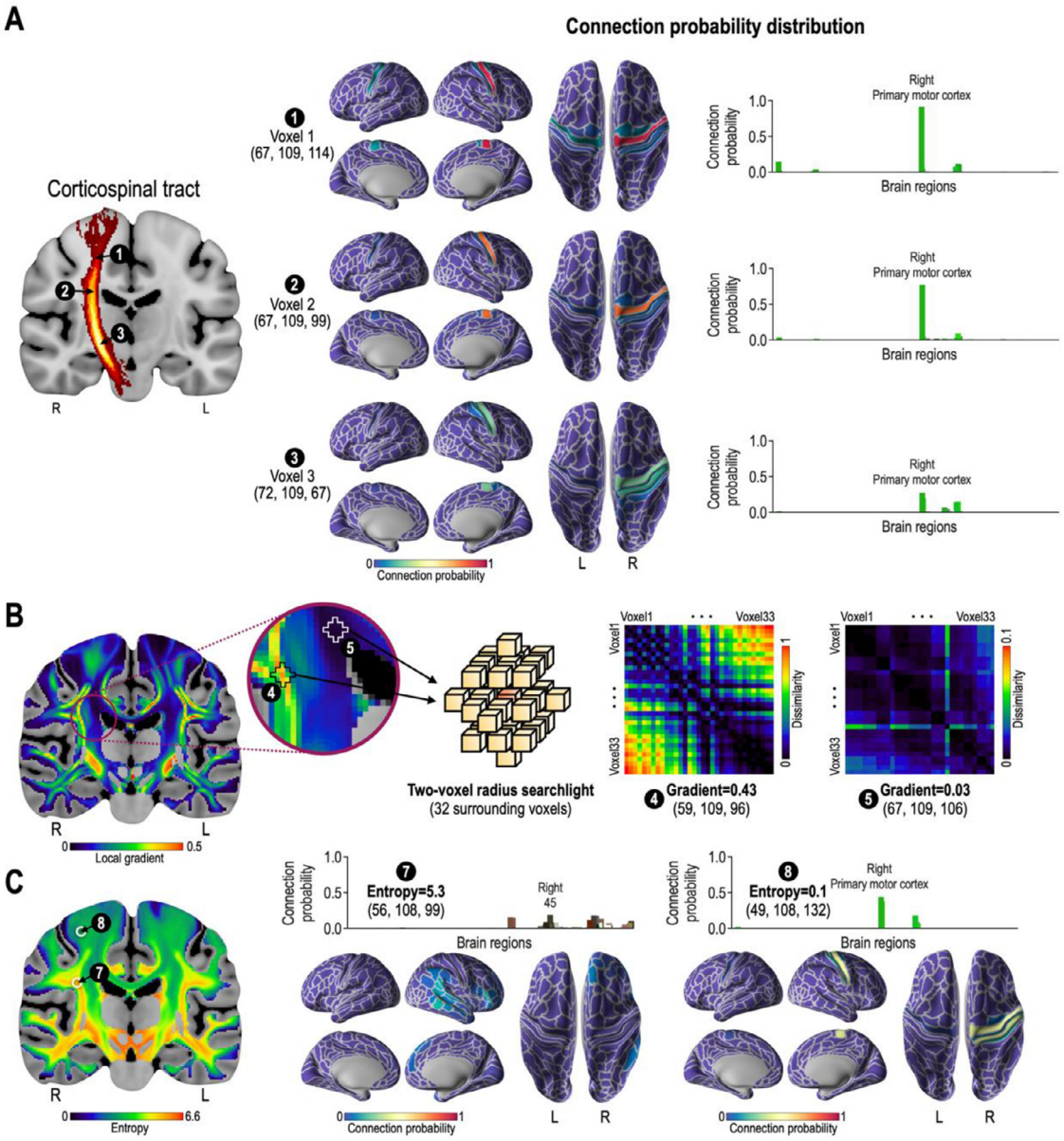

Fig. 1. Example of connection distributions in the white matter. (A) shows cortical connection distributions (with 360 cortical regions) at three voxels (1–3) within the corticospinal tract. The connection probability of cortical regions from the three voxels is displayed on the cortical surface and a bar chart. Cortical connection probability is the ratio of the number of streamlines projected to the cortical regions from the voxel versus the total number of streamlines generated at the voxel. Even at the same cortico-spinal tract, the white matter voxels show slightly different cortical connection probability along the path. (B) The connection local-gradient map shows the local gradient of connection distributions among adjacent voxels in the white matter. A high local gradient at a voxel indicates that the voxel shows high connection distribution dissimilarity with its 32 surrounding voxels. High local gradients of connection distributions are found in the midline of the white matter than in the peripheral part. Voxels 4 and 5 have high and low gradients of cortical connection patterns. (C) The connection entropy map shows the degree of uniform cortical connection from each voxel. A high entropy at a voxel indicates that streamlines passing through the white matter voxel connect the diverse cortical regions with more or less uniform connection probability (voxel 7, for example). By contrast, a low entropy indicates that the white matter voxel contains streamlines connecting to focal cortical regions (e.g., voxel 8).

(Smith et al., 2006). The TBSS skeletons were mostly located at the boundary of the connection labels (pCLM). The location of higher pCGM and pCEM overlaps with the boundary of pCLM, especially in the medial part of the brain.

4. Discussion

How axonal fibers are wired has been a long-standing issue in brain science. It has been dealt with as an organization of the information pathway from the network science perspective (Bullmore and Sporns, 2012; Hagmann et al., 2007). Since the information pathway has been implemented in the physical white matter space, the current study focuses on how the fiber bundles occupy this space. By exploring the voxel-wise distribution of cortical connections, we analyzed and visualized the wiring structure in the white matter space surrounded by the folding walls of the gray matter. When simplified, the voxel-wise exploration of structured wiring makes it an accessible problem since diverse fibers wiring cortical regions or subcortical regions are reflected in the connection distribution pattern at each white matter voxel.

Quantitative evaluation of the white matter properties has mostly been done by voxel-by-voxel analysis of the diffusion anisotropy or diffusivity (e.g., Park, 2005), either using a voxel-based processing of spatial

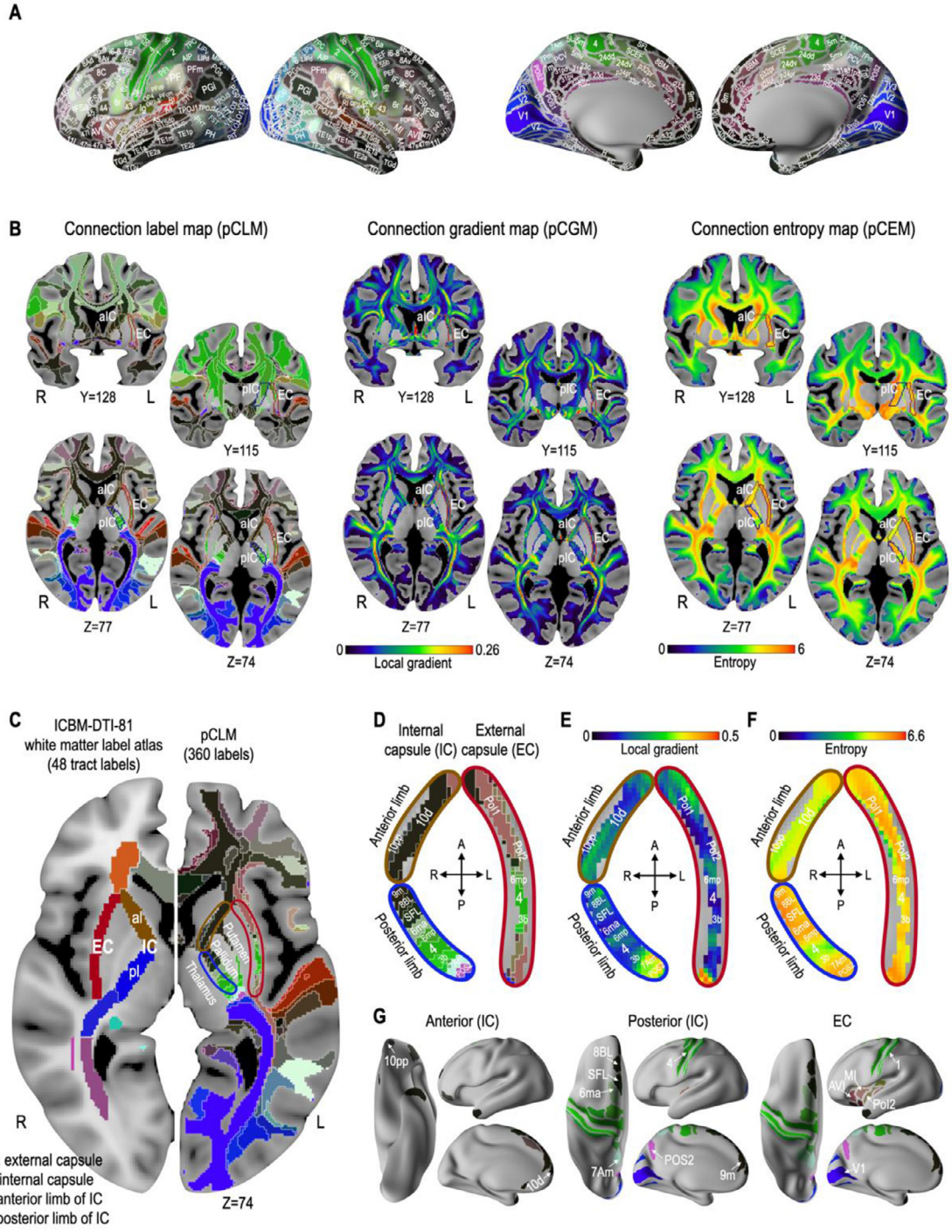

Fig. 2. Connection label, gradient, and entropy representations in the internal and external capsules. (A) The 360 cortical regions used in the current study are displayed in color over the cortical surface. The cortical colors are used to identify the corresponding white matter voxel labels (pCLM). B) Based on the connection distribution, a populational connection label map (pCLM), a connection (local-) gradient map (pCGM), and a connection entropy map (pCEM) were derived. The connection label map that indicates the maximal probability of connection at each voxel shows precise parcellations of the white matter according to corresponding cortical regions. (C) In contrast to the ICBM-DTI-81(see text), the internal capsule (IC) was subdivided into more detailed parcels; the anterior limb into the orbital and polar frontal cortices and posterior limb into diverse connections from the dorsolateral prefrontal cortex, supplementary motor areas, somatosensory and motor cortex, superior parietal cortex, and early visual cortex. The external capsule (EC) is also parcellated into multiple cortical connection areas. (D–F) display connection label, local gradient, connection entropy at each voxel of the IC and EC. (G) Target cortical regions corresponding to the labels in the IC and EC are presented on the cortical surface.

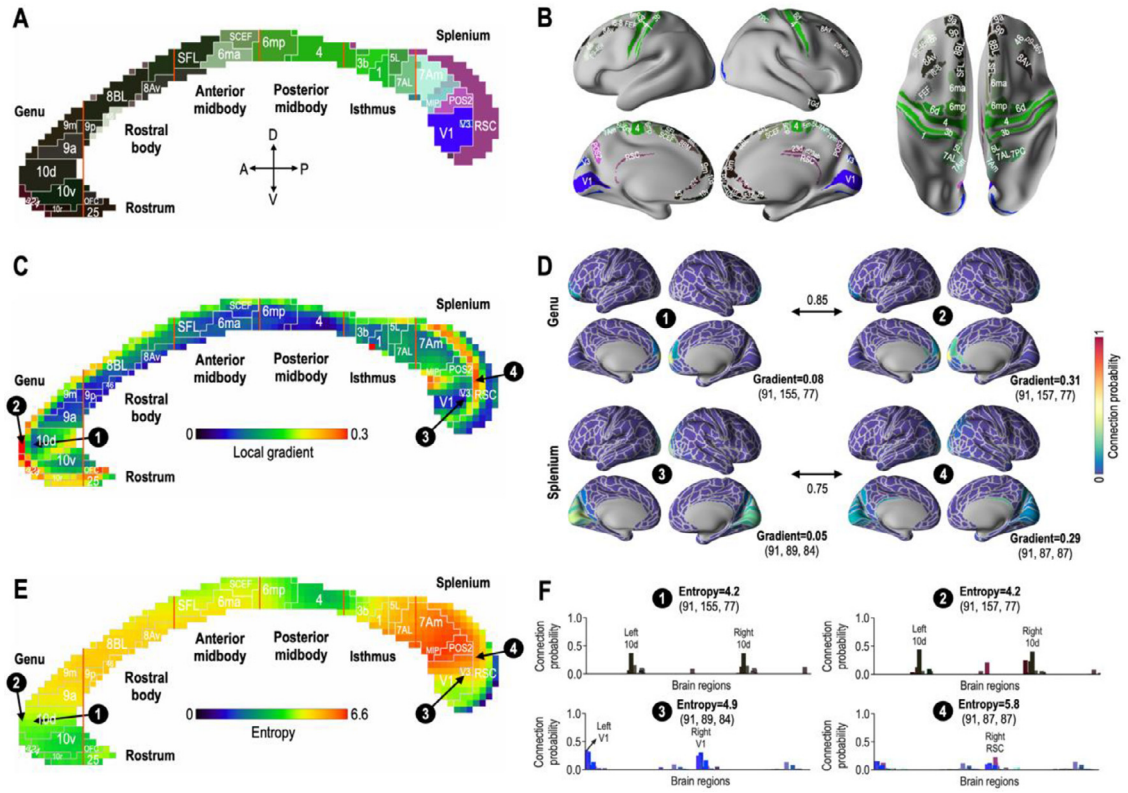

Fig. 3. Connection labels, gradient, and entropy representations in the corpus callosum. (A) The corpus callosum (CC) is parcellated according to its connection with cortical regions. (B) Connection labels of the CC are displayed on the cortical surface. (C) shows the local-gradient map at the CC with low local-gradient voxels (voxels 1 and 3) and high local-gradient voxels (voxels 2 and 4) in the genu and splenium. (D) The corresponding cortical connection distribution at those four voxels shows similar patterns of cortical connections within the same region of CC (i.e., voxels 1 and 2 at the genu and voxels 3 and 4 at the isthmus). However, depending on the precise location, it shows different local-gradient. (E) The connection entropy map is displayed. (F) The connection distribution at the same voxels (1–4) is displayed with the probability of the connection in the bar plot and their entropy.

processing (Park et al., 2003) or a tract-based spatial statistics (TBSS) approach (Smith et al., 2006). These anisotropic properties of water molecules are used to characterize brain diseases, such as schizophrenia (Kubicki et al., 2007; Kubicki et al., 2005; Park et al., 2004b) and cerebral palsy (Lee et al., 2017;Lee et al., 2011). The current connection distribution map further identifies white matter connection structures at each voxel to link the local white matter properties and their contribution to the cortical regions. It differed from previous studies that focused on the connectivity-based "parcellation" of local gray matter regions such as the thalamus (Behrens et al., 2003; Johansen-Berg et al., 2005; Lambert et al., 2017), medial frontal cortex (Johansen-Berg et al., 2004), and cerebellar cortex (van Baarsen et al., 2016), or white matter tracts, such as the CC (Chao et al., 2009; Park et al., 2008). These parcellation studies did not present the precise distribution of cortical connections at each voxel.

The connection distribution map in the current study provides the landscape of voxel-specific distribution of cortical connections, which differs according to its location, even in the same fiber pathway, for example, different cortical connections at voxels in the corticospinal tract of the white matter (Fig. 1). By taking advantage of the connection distribution, we were able to derive the most probable and the second most probable cortical label maps (pCLM), the connection gradient (pCGM), and the entropy of connection distribution (pCEM) to infer the spatial organization of the white matter. The local gradient indicates divergence in connection distributions in the connection landscape. The voxels with a high local gradient were located along the white matter's medial plane (skeleton) (See the Supplementary Fig. S6). The entropy reflects the uncertainty of the voxel interconnects with distributed cortical regions; a higher entropy indicates more diverse connections with a more uniform probability of connectivity strengths. High entropy was observed in the lower part of the brain and the middle line of the major white matter pathways, such as the forceps minor, anterior thalamic radiation, superior longitudinal fasciculus, and corticospinal tract. The high-entropy regions can be regarded as spatial hubs because various directional streamlines diverge from these high-entropy voxels.

The wiring structure of white matter was prominent in the connection-based label map. When we examined the major streamline bundles, we found some generalizable structure of wiring, represented in the three axes of partitioning in terms of cortical connections: medial-lateral, anterior-posterior, and the ventral-dorsal directions (Fig. 6). The internal and external capsules' connection distribution maps and label maps showed gradient wiring along with the anterior-posterior and medial-lateral directions. The CC, which connects the interhemispheric cortical regions of the brain, showed the anterior-posterior and ventral-dorsal directional wiring structure. These directionalities may be associated with interhemispheric, posterior-to-anterior, and inferior-to-superior information flows in the brain system. We briefly review the major streamline bundles and their wiring organization below.

4.1. Internal and external capsules

The anterior limb of the internal capsule contains streamlines that are mostly connected to the orbital and polar frontal cortical areas. The anterior limb extends to the posterior limb in containing streamlines to the frontal cortex. In contrast, the posterior limb of the internal capsule is composed of streamlines connected to the frontal, sensorimotor, parietal, and occipital cortices more precisely than a previous dif-

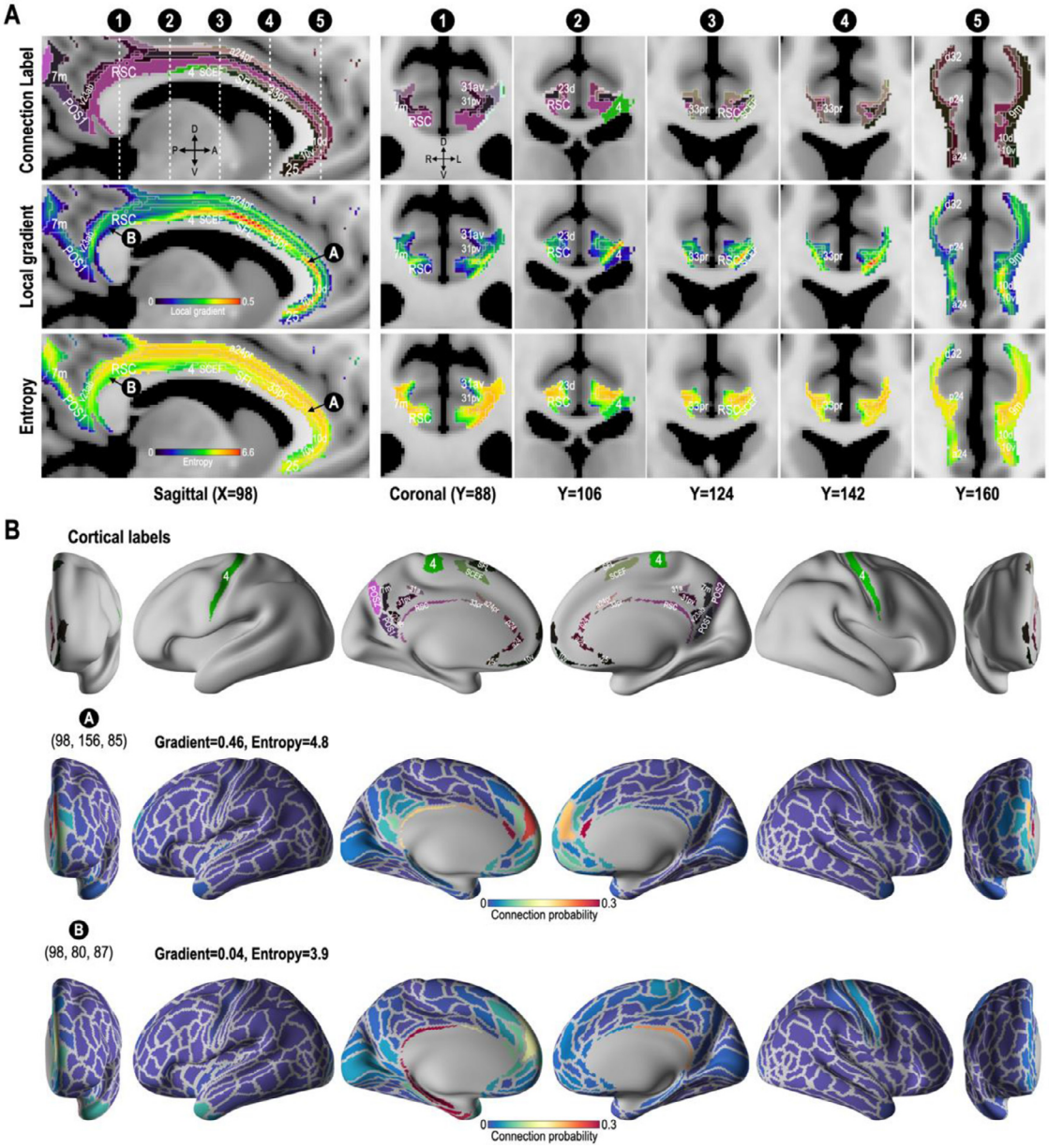

Fig. 4. Populational connection label, gradient, and entropy maps of the cingulum bundle. (A) The connection label map (top row), local-gradient map (middle row), and the entropy map (bottom row) are shown in the sagittal and coronal slices (at the coronal slice positions of 1–5). The colors in the connection label map indicate the cortical region label, annotated with the white text. (B) shows the primary cortical labels that the cingulum bundle connects (top row). The second and third rows of (B) show cortical connection probability corresponding to the two voxels A (high gradient and high entropy) and B (low gradient and low entropy) on the cortical surface. The connection label map shows subdivisions of the cingulum bundle according to cortical connection. The local-gradient map (middle row) shows a high gradient of connectivity distributions at the ventral part of the cingulum bundle. The entropy map generally shows high entropy of connectivity distribution in the cingulum bundle.

fusion MRI study (Jellison et al., 2004). It has been known that efferent fibers such as the corticobulbar tract (Yim et al., 2013), corticospinal tract (Kim et al., 2008), superior thalamic radiation (Chowdhury et al., 2010), parieto-pontocerebellar tract, and occipito-ponto-cerebellar tract (Kamali et al., 2010) pass through the posterior limb. The external capsular structure is subdivided medially and laterally.

Anatomically, the external capsular structure is located between the putamen medially and the claustrum laterally, but includes an extreme capsule separating the claustrum from the insula due to limitations in the image resolution (Alexander et al., 2020). Nevertheless, our atlas subdivided the EC medially and laterally. Specifically, streamlines passing through the medial part of the anterior EC are connected to the frontal and somatosensory motor regions, whereas streamlines passing through the lateral part of the posterior EC are connected to the insular areas (Fig. 2D).

These results outline the connection structures of the white matter that have not been shown in standard white matter atlases that were classified based on major fiber bundles (Hua et al., 2008; Mori et al., 2008; Wakana et al., 2007).

4.2. *Interhemispheric connections: corpus callosum*

The major interhemispheric fibers pass through the corpus callosum (CC) along the anterior-posterior direction in callosal cartography based on the cortical connection. It also shows the dorsal-ventral directional positioning of the streamlines. Streamlines interconnecting the dorsal

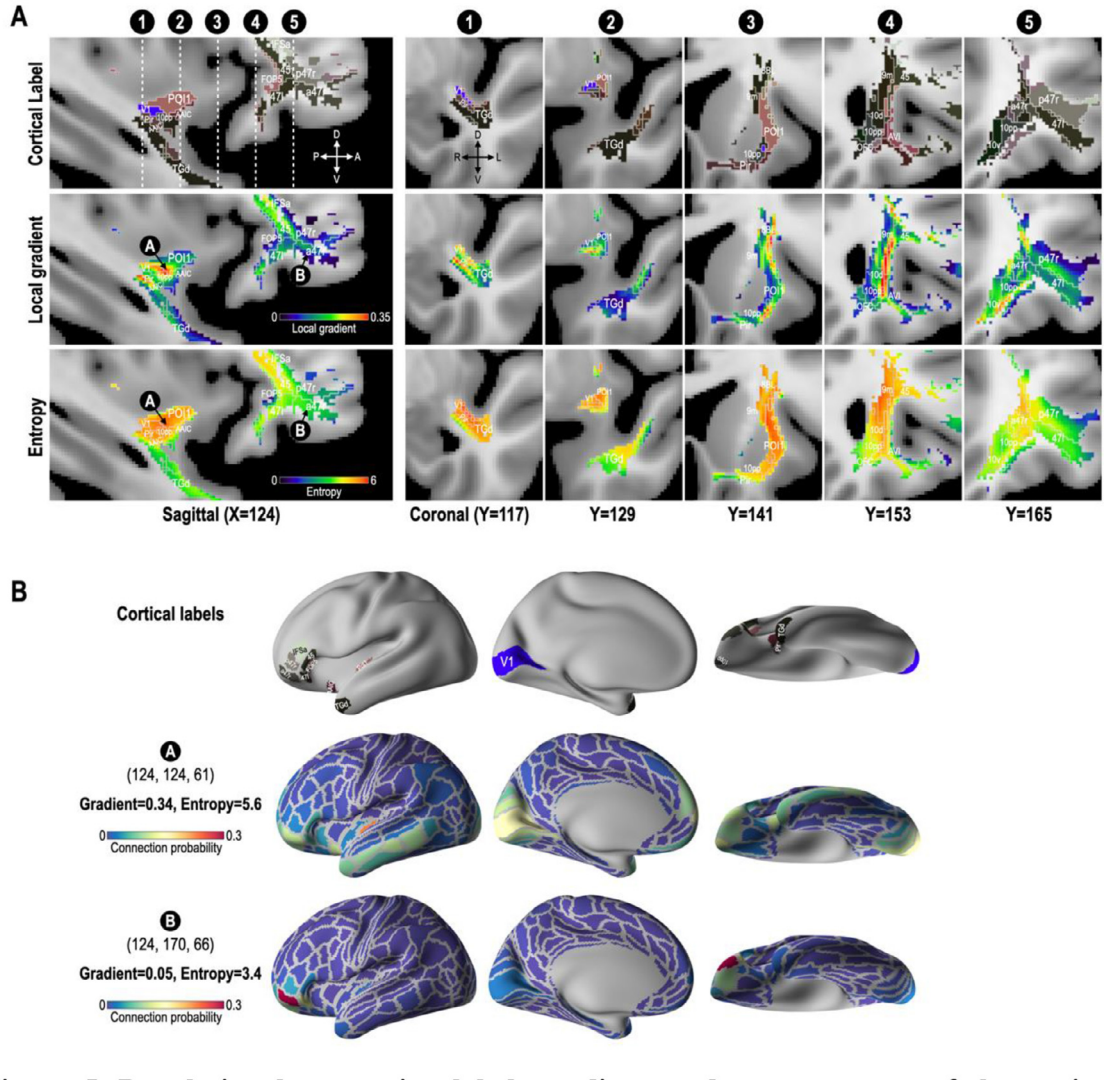

Fig. 5. Populational connection label, gradient, and entropy maps of the uncinate fasciculus tract. (A) The connection label map (top panel), local-gradient map (middle panel), and the entropy map (bottom panel) are displayed. The connection label map shows cortical subdivisions of the uncinated fasciculus that connects the orbital and polar frontal cortex, medial prefrontal regions, and lateral temporal cortex. (B) Connection labels of the uncinate fasciculus tract and the cortical connection probability at the voxel A (high gradient and high entropy) and voxel B (low gradient and low entropy) are displayed on the cortical surface.

or medial cortical lobes pass through the dorsal region of the CC, while streamlines from the lateral cortical lobes pass through the ventral part of the CC (Park et al., 2008). The current study provides a more sophisticated clustering of the CC. The dorsal parts of the genu and splenium show uniform distributions of vast cortical connections (Fig. 3E), which may act as a hub of pathways in which diverse brain regions cross at those regions. We speculate that the uniform-distributed connections in the genu and splenium may be associated with the highest density of thin fibers (<0.4) situated in the genu and anterior splenium (Raybaud, 2010) in terms of packing all the wires to diverse cortical regions within the limited cross-sectional area.

4.3. Anterior-posterior connection: cingulum bundle

The cingulum is spatially organized to interconnect heterogeneous and complex anatomical pathways for diverse functions in multiple areas (Kollias, 2009; Schmahmann et al., 2007). Overall, these results support the role of the cingulate cortex as a cornerstone in higher-order cognitive functions such as attention (Gusnard et al., 2001; Hahn et al., 2007), emotion (Bush et al., 2000; Maddock et al., 2003), and memory (Valenstein et al., 1987).

As shown in Fig. 4, two distinct subdivisions were observed in the cingulum tract. Specifically, the anterior part of the cingulum contained streamlines connecting the anterior cingulate and medial prefrontal cortex. In contrast, the posterior part was primarily occupied with streamlines connecting the posterior cingulate cortex. A high transition gradient was observed along the anterior-posterior axis of the cingulum bundle, except for the regions behind the splenium of the CC. The connection entropy is mostly high across the cingulum tract, indicating that the cingulum tract mediates diverse connections.

4.4. Medial-lateral connection: uncinate fasciculus (UF)

The uncinate fasciculus fibers interconnect the orbitofrontal cortex with the anterior temporal lobes (Von Der Heide et al., 2013). The UF is associated with the ventral stream of language processing that mediates higher-level language information among the middle, temporal and ventrolateral prefrontal cortices (Saur et al., 2008). Consistent with previous findings (Catani et al., 2002; Kier et al., 2004), the anterior aspect of the left UF contained streamlines linked to the prefrontal cortical regions, whereas the lateral aspect contained streamlines linked to the insula and anterior temporal pole. Fibers passing through the anterior

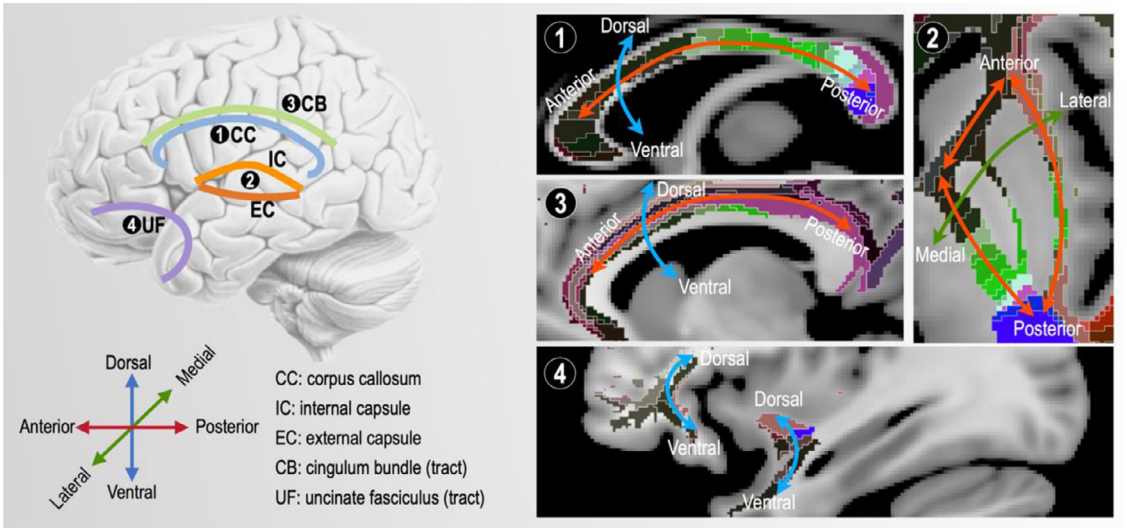

Fig. 6. Summary of cortical connections within the white matter. Although the wiring of the fiber bundles in the white matter has more than one directional connection and the complexity of the wiring is very high, we simplified the wiring pattern of the major fiber bundles according to primary axes in the three-dimensional space. White matter fiber streamlines passing through the internal and external capsules, corpus callosum, and cingulum bundle are principally wired along the anterior-to-posterior axis of the brain. White matter streamlines passing through the corpus callosum, cingulum tract, and uncinate fasciculus tract are wired along the dorsal-to-ventral axis. White matter streamlines passing through the external capsule are wired along the lateral-to-medial axis. The white matter connections are spatially organized to wire all the necessary connections with cortical gray matter regions in the three-dimensional space.

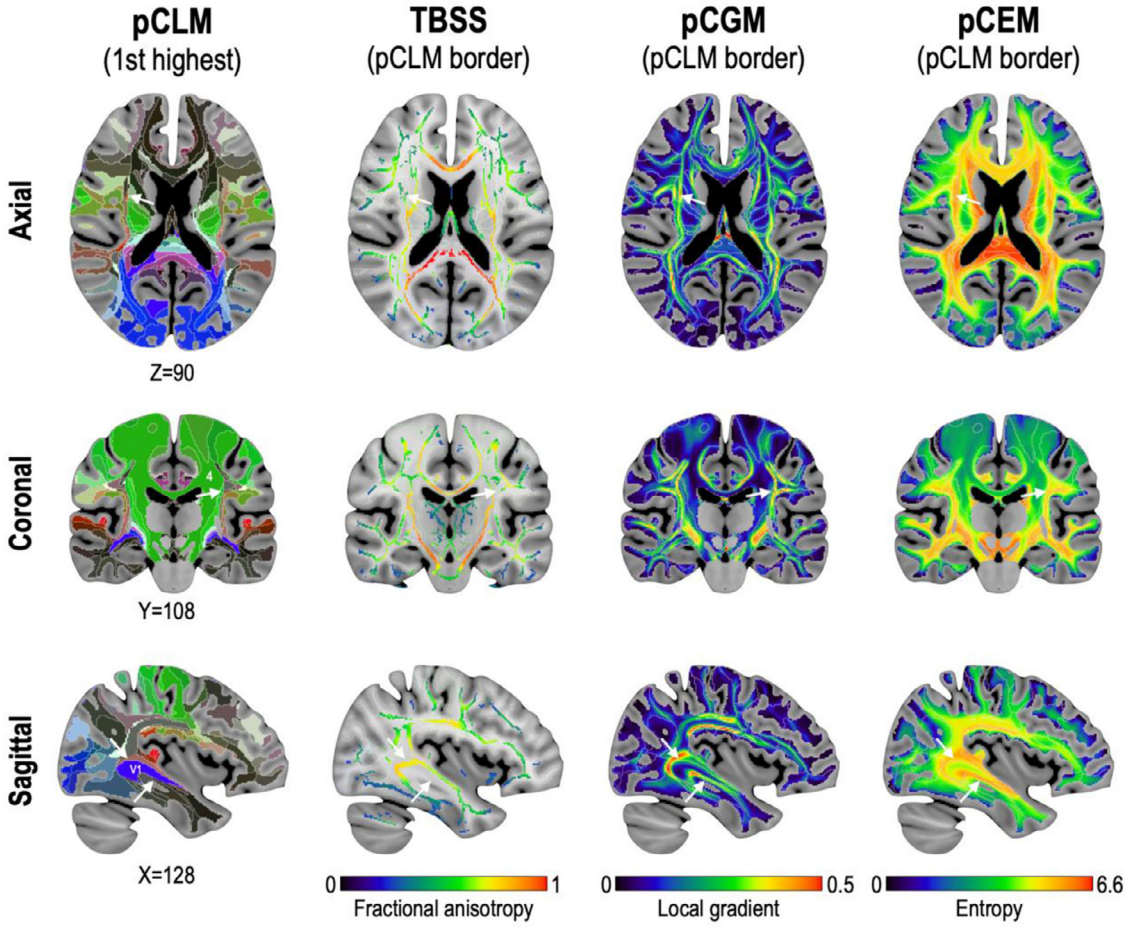

Fig. 7. Comparison of the tract-based spatial statistics (TBSS) skeleton with the pCLM (the highest connection probability), pCGM, and pCEM, displayed with pCLM border lines in white. The pCLM borders are presented to show each cluster's extent and demonstrate the limitation of the projection of neighboring voxels' diffusion properties to a skeleton point in the TBSS. The major streamline bundles' skeleton in the TBSS overlaps grossly with the pCLM border, indicating that the neighboring voxels perpendicular to a point in the skeleton of the TBSS may contain streamlines of different cortical connections and thus may induce the specificity problem.

temporal lobe are more likely to be connected to the insula and frontal operculum, lateral temporal cortex, and primary visual cortex. In contrast, voxels in the inferior frontal lobe are more likely to be connected to the inferior, orbital, and polar frontal cortex, and the dorsolateral prefrontal cortex (Fig. 5).

4.5. Structured gradient in the connection organization

A spatial order exists in the brain wiring in the three-dimensional white matter space; wiring in the anterior-posterior direction, ventral-dorsal direction, and medial and lateral directions are the major axes of wiring. The pattern of anterior-posterior and ventral-dorsal directional positioning in CC has already been discussed by Park et al. (2008). We also found these ordered positioning in the internal and external capsules, which showed a medial-lateral directional connection. The ventral-dorsal positioning of cortical fibers is found in the uncinate fasciculus along the ventral pathway between the temporal cortex and the inferior frontal gyrus (Ebeling and von Cramon, 1992; Perani et al., 2011). Anterior-posterior directional gradients are observed in the cingulum bundles, separating the anterior and posterior parts (Brodmann, 1909; Vogt, 1993). The wiring in the three-dimensional space is graded according to the positions of the cortical regions that the streamlines interconnect. These types of gradients are essential for packing very complex wires within a limited white matter space (Martino et al., 2011). All this wiring could be interpreted in terms of the development of the cortical region and its interconnecting white matter. The white matter may have been patterned to support the continuous folding of the cortical sulcus and gyrus, thus improving inter-regional connections. (Garcia et al., 2018; Tallinen et al., 2016; Van Essen, 2020).

The gradient wiring slightly differs from that of the functional gradients in previous studies (Guell et al., 2018; Huntenburg et al., 2018; Margulies et al., 2016; Paquola et al., 2019; Wang, 2020; Yang et al., 2020). Functional gradients represent continuous transitions in functional connectivity patterns, without specific consideration of the physical space. Further studies remain to associate functional gradients and current wiring patterns within the space.

Of note, we compared the current analysis results, such as local gradients, with the skeleton of a TBSS approach (Smith et al., 2006) which has been widely used to analyze diffusion properties (See Fig. 7). All the voxel properties (fractional anisotropy or diffusivity) are perpendicularly projected to neighboring points in a skeleton, which is the medial line of the white matter. The TBSS assumes that voxels projecting to a skeleton point are homogeneous. However, as seen in the previous figures, the medial lines mostly bordered the connection profiles. It is a diverging region where diverse directional streamlines share a position temporally but later diverge to various cortical areas. In this respect, TBSS is limited to representing the specificity of each voxel and may merge heterogeneous streamline properties into a skeleton. This issue has already been raised in a previous study (Edden and Jones, 2011; Schwarz et al., 2014; Zalesky, 2011).

The current study explaining a connection distribution map generated by a state-of-art method of diffusion MRI analysis is mainly descriptive. Unfortunately, the white matter parcellation for the major fiber bundles comparable to the current study is rarely found in histology studies. Therefore, the connection distribution map of the human should be validated, particularly at the histological level using various circuit tracing techniques such as anterograde and retrograde tracing.

In summary, we presented a connection distribution map to identify the connection structures of the white matter at the voxel level. Understanding the connection structure of the white matter on a voxel-wise level may help decide the appropriate treatment, such as surgical resection of the white matter voxels, to reduce the risk of functional loss in the brain. The connection distribution, gradient and entropy information provided in the current study are particularly important for defining the margin of each lesion in the presurgical planning of patients with white matter lesions (Park et al., 2004a). We expect that the current atlas will assist researchers in identifying the connection organizations of white matter with ease and proficiency.

Data and code availability statements

All MRI data (DTI and T1) is available from the Human Connectome Project (HCP) 1200 Subjects release image and behavioral data (https://www.humanconnectome.org/study/hcp-young-adult/document/1200-subjects-data-release). We received permission to access the HCP database to use the public data, and it does not need any consent from the individuals for the current study. The suggested connection distribution map in the current study is available at http://neuroimage.yonsei.ac.kr:3000. Full access to the connection distribution map and code will be granted on requestion through email.

Credit authorship contribution statement

Dongha Lee: Conceptualization, Methodology, Formal analysis, Software, Writing – original draft, Data curation. **Hae-Jeong Park:** Conceptualization, Methodology, Software, Writing – review & editing, Project administration, Funding acquisition.

Acknowledgments

This research was supported by Brain Research Program through the National Research Foundation of Korea (NRF) funded by the Ministry of Science and ICT (NRF-2017M3C7A1049051) to HJP, and by KBRI basic research program through Korea Brain Research Institute funded by Ministry of Science and ICT (21-BR-05-01) to DL.

Supplementary materials

Supplementary material associated with this article can be found, in the online version, at doi:10.1016/j.neuroimage.2022.119167.

References

Alexander, B., Yang, J.Y., Yao, S.H.W., Wu, M.H., Chen, J., Kelly, C.E., Ball, G., Matthews, L.G., Seal, M.L., Anderson, P.J., Doyle, L.W., Cheong, J.L.Y., Spittle, A.J., Thompson, D.K., 2020. White matter extension of the Melbourne children's regional Infant brain atlas: M-CRIB-WM. Hum. Brain Mapp. 41, 2317–2333.

Ashburner, J., 2007. A fast diffeomorphic image registration algorithm. Neuroimage 38, 95–113.

Bajada, C.J., Costa Campos, L.Q., Caspers, S., Muscat, R., Parker, G.J.M., Lambon Ralph, M.A., Cloutman, L.L., Trujillo-Barreto, N.J., 2020. A tutorial and tool for exploring feature similarity gradients with MRI data. Neuroimage 221, 117140.

Basser, P.J., Mattiello, J., LeBihan, D., 1994. MR diffusion tensor spectroscopy and imaging. Biophys. J. 66, 259–267.

Behrens, T.E., Berg, H.J., Jbabdi, S., Rushworth, M.F., Woolrich, M.W., 2007. Probabilistic diffusion tractography with multiple fibre orientations: what can we gain? Neuroimage 34, 144–155.

Behrens, T.E., Johansen-Berg, H., Woolrich, M.W., Smith, S.M., Wheeler-Kingshott, C.A., Boulby, P.A., Barker, G.J., Sillery, E.L., Sheehan, K., Ciccarelli, O., Thompson, A.J., Brady, J.M., Matthews, P.M., 2003. Non-invasive mapping of connections between human thalamus and cortex using diffusion imaging. Nat. Neurosci. 6, 750–757.

Brodmann, K., 1909. Vergleichende Lokalisationslehre der Grosshirnrinde in Ihren Prinzipien Dargestellt auf Grund des Zellenbaues. Barth.

Bullmore, E., Sporns, O., 2012. The economy of brain network organization. Nat. Rev. Neurosci. 13, 336–349.

Bush, G., Luu, P., Posner, M.I., 2000. Cognitive and emotional influences in anterior cingulate cortex. Trends Cogn. Sci. 4, 215–222.

Catani, M., Howard, R.J., Pajevic, S., Jones, D.K., 2002. Virtual *in vivo* interactive dissection of white matter fasciculi in the human brain. Neuroimage 17, 77–94.

Chao, Y.P., Cho, K.H., Yeh, C.H., Chou, K.H., Chen, J.H., Lin, C.P., 2009. Probabilistic topography of human corpus callosum using cytoarchitectural parcellation and high angular resolution diffusion imaging tractography. Hum. Brain Mapp. 30, 3172–3187.

Chowdhury, F., Haque, M., Sarkar, M., Ara, S., Islam, M., 2010. White fiber dissection of brain; the internal capsule: a cadaveric study. Turk. Neurosurg. 20, 314–322.

Ebeling, U., von Cramon, D., 1992. Topography of the uncinate fascicle and adjacent temporal fiber tracts. Acta Neurochir. 115, 143–148 (Wien).

Edden, R.A., Jones, D.K., 2011. Spatial and orientational heterogeneity in the statistical sensitivity of skeleton-based analyses of diffusion tensor MR imaging data. J. Neurosci. Methods 201, 213–219.

Fiedler, M., 1973. Algebraic connectivity of graphs. Czechoslov. Math. J. 1973, 298–305.

Garcia, K.E., Kroenke, C.D., Bayly, P.V., 2018. Mechanics of cortical folding: stress, growth and stability. Philos. Trans. R. Soc. Lond. B Biol. Sci. 373, 20170321.

Glasser, M.F., Coalson, T.S., Robinson, E.C., Hacker, C.D., Harwell, J., Yacoub, E., Ugurbil, K., Andersson, J., Beckmann, C.F., Jenkinson, M., Smith, S.M., Van Essen, D.C., 2016. A multi-modal parcellation of human cerebral cortex. Nature 536, 171–178.
Guell, X., Schmahmann, J.D., Gabrieli, J., Ghosh, S.S., 2018. Functional gradients of the cerebellum. eLife 7, e36652.
Gusnard, D.A., Raichle, M.E., Raichle, M.E., 2001. Searching for a baseline: functional imaging and the resting human brain. Nat. Rev. Neurosci. 2, 685–694.
Hagmann, P., Kurant, M., Gigandet, X., Thiran, P., Wedeen, V.J., Meuli, R., Thiran, J.P., 2007. Mapping human whole-brain structural networks with diffusion MRI. PLoS One 2, e597.
Hahn, B., Ross, T.J., Stein, E.A., 2007. Cingulate activation increases dynamically with response speed under stimulus unpredictability. Cereb. Cortex 17, 1664–1671.
Hernandez-Fernandez, M., Reguly, I., Jbabdi, S., Giles, M., Smith, S., Sotiropoulos, S.N., 2019. Using GPUs to accelerate computational diffusion MRI: from microstructure estimation to tractography and connectomes. Neuroimage 188, 598–615.
Hua, K., Zhang, J., Wakana, S., Jiang, H., Li, X., Reich, D.S., Calabresi, P.A., Pekar, J.J., van Zijl, P.C., Mori, S., 2008. Tract probability maps in stereotaxic spaces: analyses of white matter anatomy and tract-specific quantification. Neuroimage 39, 336–347.
Huntenburg, J.M., Bazin, P.L., Margulies, D.S., 2018. Large-scale gradients in human cortical organization. Trends Cogn. Sci. 22, 21–31.
Jbabdi, S., Sotiropoulos, S.N., Savio, A.M., Grana, M., Behrens, T.E., 2012. Model-based analysis of multishell diffusion MR data for tractography: how to get over fitting problems. Magn. Reson. Med. 68, 1846–1855.
Jellison, B.J., Field, A.S., Medow, J., Lazar, M., Salamat, M.S., Alexander, A.L., 2004. Diffusion tensor imaging of cerebral white matter: a pictorial review of physics, fiber tract anatomy, and tumor imaging patterns. AJNR Am. J. Neuroradiol. 25, 356–369.
Johansen-Berg, H., Behrens, T.E., Robson, M.D., Drobnjak, I., Rushworth, M.F., Brady, J.M., Smith, S.M., Higham, D.J., Matthews, P.M., 2004. Changes in connectivity profiles define functionally distinct regions in human medial frontal cortex. Proc. Natl. Acad. Sci. U. S. A. 101, 13335–13340.
Johansen-Berg, H., Behrens, T.E., Sillery, E., Ciccarelli, O., Thompson, A.J., Smith, S.M., Matthews, P.M., 2005. Functional-anatomical validation and individual variation of diffusion tractography-based segmentation of the human thalamus. Cereb. Cortex 15, 31–39.
Kamali, A., Kramer, L.A., Frye, R.E., Butler, I.J., Hasan, K.M., 2010. Diffusion tensor tractography of the human brain cortico-ponto-cerebellar pathways: a quantitative preliminary study. J. Magn. Reson. Imaging 32, 809–817.
Kier, E.L., Staib, L.H., Davis, L.M., Bronen, R.A., 2004. MR imaging of the temporal stem: anatomic dissection tractography of the uncinate fasciculus, inferior occipitofrontal fasciculus, and Meyer's loop of the optic radiation. AJNR Am. J. Neuroradiol. 25, 677–691.
Kim, Y.H., Kim, D.S., Hong, J.H., Park, C.H., Hua, N., Bickart, K.C., Byun, W.M., Jang, S.H., 2008. Corticospinal tract location in internal capsule of human brain: diffusion tensor tractography and functional MRI study. Neuroreport 19, 817–820.
Kollias, S., 2009. Parcelation of the White Matter Using DTI: Insights Into the Functional Connectivity of the Brain. SAGE Publications Sage UK: London, England.
Kubicki, M., McCarley, R., Westin, C.F., Park, H.J., Maier, S., Kikinis, R., Jolesz, F.A., Shenton, M.E., 2007. A review of diffusion tensor imaging studies in schizophrenia. J. Psychiatr. Res. 41, 15–30.
Kubicki, M., Park, H., Westin, C.F., Nestor, P.G., Mulkern, R.V., Maier, S.E., Niznikiewicz, M., Connor, E.E., Levitt, J.J., Frumin, M., Kikinis, R., Jolesz, F.A., McCarley, R.W., Shenton, M.E., 2005. DTI and MTR abnormalities in schizophrenia: analysis of white matter integrity. Neuroimage 26, 1109–1118.
Lambert, C., Simon, H., Colman, J., Barrick, T.R., 2017. Defining thalamic nuclei and topographic connectivity gradients *in vivo*. Neuroimage 158, 466–479.
Lee, D., Pae, C., Lee, J.D., Park, E.S., Cho, S.R., Um, M.H., Lee, S.K., Oh, M.K., Park, H.J., 2017. Analysis of structure-function network decoupling in the brain systems of spastic diplegic cerebral palsy. Hum. Brain Mapp. 38, 5292–5306.
Lee, J.D., Park, H.J., Park, E.S., Oh, M.K., Park, B., Rha, D.W., Cho, S.R., Kim, E.Y., Park, J.Y., Kim, C.H., Kim, D.G., Park, C.I., 2011. Motor pathway injury in patients with periventricular leucomalacia and spastic diplegia. Brain 134, 1199–1210.
Li, L., Rilling, J.K., Preuss, T.M., Glasser, M.F., Hu, X., 2012. The effects of connection reconstruction method on the interregional connectivity of brain networks via diffusion tractography. Hum. Brain Mapp. 33, 1894–1913.
Maddock, R.J., Garrett, A.S., Buonocore, M.H., 2003. Posterior cingulate cortex activation by emotional words: fMRI evidence from a valence decision task. Hum. Brain Mapp. 18, 30–41.
Margulies, D.S., Ghosh, S.S., Goulas, A., Falkiewicz, M., Huntenburg, J.M., Langs, G., Bezgin, G., Eickhoff, S.B., Castellanos, F.X., Petrides, M., Jefferies, E., Smallwood, J., 2016. Situating the default-mode network along a principal gradient of macroscale cortical organization. Proc. Natl. Acad. Sci. U. S. A. 113, 12574–12579.
Martino, J., De Witt Hamer, P.C., Vergani, F., Brogna, C., de Lucas, E.M., Vazquez-Barquero, A., Garcia-Porrero, J.A., Duffau, H., 2011. Cortex-sparing fiber dissection: an improved method for the study of white matter anatomy in the human brain. J. Anat. 219, 531–541.
Mori, S., Oishi, K., Jiang, H., Jiang, L., Li, X., Akhter, K., Hua, K., Faria, A.V., Mahmood, A., Woods, R., Toga, A.W., Pike, G.B., Neto, P.R., Evans, A., Zhang, J., Huang, H., Miller, M.I., van Zijl, P., Mazziotta, J., 2008. Stereotaxic white matter atlas based on diffusion tensor imaging in an ICBM template. Neuroimage 40, 570–582.
Oishi, K., Zilles, K., Amunts, K., Faria, A., Jiang, H., Li, X., Akhter, K., Hua, K., Woods, R., Toga, A.W., Pike, G.B., Rosa-Neto, P., Evans, A., Zhang, J., Huang, H., Miller, M.I., van Zijl, P.C., Mazziotta, J., Mori, S., 2008. Human brain white matter atlas: identification and assignment of common anatomical structures in superficial white matter. Neuroimage 43, 447–457.
Paquola, C., Vos De Wael, R., Wagstyl, K., Bethlehem, R.A.I., Hong, S.J., Seidlitz, J., Bullmore, E.T., Evans, A.C., Misic, B., Margulies, D.S., Smallwood, J., Bernhardt, B.C., 2019. Microstructural and functional gradients are increasingly dissociated in transmodal cortices. PLoS Biol. 17, e3000284.
Park, H.J., 2005. Quantification of white matter using diffusion-tensor imaging. Int. Rev. Neurobiol. 66, 167–212.
Park, H.J., Friston, K., 2013. Structural and functional brain networks: from connections to cognition. Science 342, 1238411.
Park, H.J., Kim, J.J., Lee, S.K., Seok, J.H., Chun, J., Kim, D.I., Lee, J.D., 2008. Corpus callosal connection mapping using cortical gray matter parcellation and DT-MRI. Hum. Brain Mapp. 29, 503–516.
Park, H.J., Kubicki, M., Shenton, M.E., Guimond, A., McCarley, R.W., Maier, S.E., Kikinis, R., Jolesz, F.A., Westin, C.F., 2003. Spatial normalization of diffusion tensor MRI using multiple channels. Neuroimage 20, 1995–2009.
Park, H.J., Kubicki, M., Westin, C.F., Talos, I.F., Brun, A., Peiper, S., Kikinis, R., Jolesz, F.A., McCarley, R.W., Shenton, M.E., 2004a. Method for combining information from white matter fiber tracking and gray matter parcellation. AJNR Am. J. Neuroradiol. 25, 1318–1324.
Park, H.J., Westin, C.F., Kubicki, M., Maier, S.E., Niznikiewicz, M., Baer, A., Frumin, M., Kikinis, R., Jolesz, F.A., McCarley, R.W., Shenton, M.E., 2004b. White matter hemisphere asymmetries in healthy subjects and in schizophrenia: a diffusion tensor MRI study. Neuroimage 23, 213–223.
Perani, D., Saccuman, M.C., Scifo, P., Anwander, A., Spada, D., Baldoli, C., Poloniato, A., Lohmann, G., Friederici, A.D., 2011. Neural language networks at birth. Proc. Natl. Acad. Sci. U. S. A. 108, 16056–16061.
Raybaud, C., 2010. The corpus callosum, the other great forebrain commissures, and the septum pellucidum: anatomy, development, and malformation. Neuroradiology 52, 447–477.
Saur, D., Kreher, B.W., Schnell, S., Kummerer, D., Kellmeyer, P., Vry, M.S., Umarova, R., Musso, M., Glauche, V., Abel, S., Huber, W., Rijntjes, M., Hennig, J., Weiller, C., 2008. Ventral and dorsal pathways for language. Proc. Natl. Acad. Sci. U. S. A. 105, 18035–18040.
Schmahmann, J.D., Pandya, D.N., Wang, R., Dai, G., D'Arceuil, H.E., de Crespigny, A.J., Wedeen, V.J., 2007. Association fibre pathways of the brain: parallel observations from diffusion spectrum imaging and autoradiography. Brain 130, 630–653.
Schwarz, C.G., Reid, R.I., Gunter, J.L., Senjem, M.L., Przybelski, S.A., Zuk, S.M., Whitwell, J.L., Vemuri, P., Josephs, K.A., Kantarci, K., Thompson, P.M., Petersen, R.C., Jack, C.R.Alzheimer's Disease Neuroimaging Initiative, 2014. Improved DTI registration allows voxel-based analysis that outperforms tract-based spatial statistics. Neuroimage 94, 65–78.
Smith, S.M., Jenkinson, M., Johansen-Berg, H., Rueckert, D., Nichols, T.E., Mackay, C.E., Watkins, K.E., Ciccarelli, O., Cader, M.Z., Matthews, P.M., Behrens, T.E., 2006. Tract-based spatial statistics: voxelwise analysis of multi-subject diffusion data. Neuroimage 31, 1487–1505.
Sporns, O., 2013. The human connectome: origins and challenges. Neuroimage 80, 53–61.
Tallinen, T., Chung, J.Y., Rousseau, F., Girard, N., Lefèvre, J., Mahadevan, L., 2016. On the growth and form of cortical convolutions. Nat. phy. 12, 588–593.
Valenstein, E., Bowers, D., Verfaellie, M., Heilman, K.M., Day, A., Watson, R.T., 1987. Retrosplenial amnesia. Brain 110 (Pt 6), 1631–1646.
van Baarsen, K.M., Kleinnijenhuis, M., Jbabdi, S., Sotiropoulos, S.N., Grotenhuis, J.A., van Cappellen van Walsum, A.M., 2016. A probabilistic atlas of the cerebellar white matter. Neuroimage 124, 724–732.
Van Essen, D.C., 2020. A 2020 view of tension-based cortical morphogenesis. Proc. Natl. Acad. Sci. U. S. A. 117, 32868–32879.
Van Essen, D.C., Ugurbil, K., Auerbach, E., Barch, D., Behrens, T.E., Bucholz, R., Chang, A., Chen, L., Corbetta, M., Curtiss, S.W., Della Penna, S., Feinberg, D., Glasser, M.F., Harel, N., Heath, A.C., Larson-Prior, L., Marcus, D., Michalareas, G., Moeller, S., Oostenveld, R., Petersen, S.E., Prior, F., Schlaggar, B.L., Smith, S.M., Snyder, A.Z., Xu, J., Yacoub, E.WU-Minn HCP Consortium, 2012. The Human Connectome Project: a data acquisition perspective. Neuroimage 62, 2222–2231.
Vogt, B.A., 1993. Structural Organization of Cingulate Cortex: Areas, Neurons, and Somatodendritic Transmitter Receptors. Birkhäuser, Boston, MA.
Von Der Heide, R.J., Skipper, L.M., Klobusicky, E., Olson, I.R., 2013. Dissecting the uncinate fasciculus: disorders, controversies and a hypothesis. Brain 136, 1692–1707.
Wakana, S., Caprihan, A., Panzenboeck, M.M., Fallon, J.H., Perry, M., Gollub, R.L., Hua, K., Zhang, J., Jiang, H., Dubey, P., Blitz, A., van Zijl, P., Mori, S., 2007. Reproducibility of quantitative tractography methods applied to cerebral white matter. Neuroimage 36, 630–644.
Wang, X.J., 2020. Macroscopic gradients of synaptic excitation and inhibition in the neocortex. Nat. Rev. Neurosci. 21, 169–178.
Witelson, S.F., 1989. Hand and sex differences in the isthmus and genu of the human corpus callosum. A postmortem morphological study. Brain 112 (Pt 3), 799–835.
Yang, S., Meng, Y., Li, J., Li, B., Fan, Y., Chen, H., Liao, W., 2020. The thalamic functional gradient and its relationship to structural basis and cognitive relevance. Neuroimage 218, 116960.
Yim, S.H., Kim, J.H., Han, Z.A., Jeon, S., Cho, J.H., Kim, G.S., Choi, S.A., Lee, J.H., 2013. Distribution of the corticobulbar tract in the internal capsule. J. Neurol. Sci. 334, 63–68.
Zalesky, A., 2011. Moderating registration misalignment in voxelwise comparisons of DTI data: a performance evaluation of skeleton projection. Magn. Reson. Imaging 29, 111–125.